Available online at www.sciencedirect.com
ScienceDirect
Carbon 44 (2006) 2973–2983
CARBON
www.elsevier.com/locate/carbon

Electro-catalytic oxidation of CO on Pt catalyst supported on carbon nanotubes pretreated with oxidative acids

Li Li, Gang Wu, Bo-Qing Xu *

Innovative Catalysis Program, Key Lab of Organic Optoelectronics and Molecular Engineering, Department of Chemistry, Tsinghua University, Beijing 100084, China

Received 9 December 2005; accepted 19 May 2006
Available online 7 July 2006

Abstract

Characteristics of nanosized Pt electro-catalyst deposited on carbon nanotubes (CNTs) were studied with CO-stripping voltammogram and chronoamperometry measurements. The CNTs were pretreated by oxidation in HNO_3, mixed $HNO_3 + H_2SO_4$ and $H_2SO_4 + K_2Cr_2O_7$ solution, respectively, to enable surface modification. Well-homogenized Pt particles (average size: ≈3 nm) were loaded onto the pretreated CNT samples by a modified colloidal method. TEM, BET, FTIR and XRD techniques were used to characterize the physicochemical properties of the pretreated CNT samples. In the electro-oxidation of CO, all the Pt/CNT samples showed lower on-set as well as peak potentials than the conventional Pt/XC-72 electro-catalyst, indicating that the Pt/CNT samples were more resistant to CO poisoning and could be superior anode electro-catalyst for the proton exchange membrane fuel cells (PEMFCs). Moreover, we found that the pretreatment of CNTs in mixed $HNO_3 + H_2SO_4$ solution was very beneficial for the performance enhancement of Pt/CNT electro-catalyst; the catalyst obtained as such gave the lowest peak potential and the highest catalytic activity for the electro-oxidation of CO. Larger amount of oxygen-containing functional groups, higher percentage of mesopores, and higher graphitic crystallinity of the pretreated CNTs were considered crucial for the performance enhancement, e.g., by strengthening the interaction between Pt nanoparticles and the CNT support and enhancing the mass diffusion in the electro-chemical reaction.

Keywords: Carbon nanotubes; Chemically modified carbons; Catalyst support; Electro-chemical properties; Chemical treatment

1. Introduction

There has been increasing interest in proton exchange membrane fuel cells (PEMFCs) as zero emission power sources [1–3]. Pure hydrogen is an ideal fuel for PEMFCs. However, the production, storage and refueling infrastructure of hydrogen are still of significant problems [4]. To avoid such difficulties, the use of hydrogen-rich synthetic gas obtained from steam-reforming or partial oxidation of alcohols or hydrocarbons can be a feasible choice [5–7]. For example, the methanol reforming results in a gas mixture of approximately 74% H_2, 25% CO_2 and 1–2% CO [8]. However, a detractor to this technology is that the presence of even a small amount of CO would result in poisoning of the hydrogen oxidation reaction occurring at the anode Pt catalyst, and consequently lower energy conversion efficiency; which is referred to as CO-poisoning effect [9,10]. Using special selective oxidation catalyst, the CO concentration in hydrogen can be reduced further to approximately 2–100 ppm. But even at this level, the CO-poisoning effect could also significantly plague the long-term performance of the PEMFC stack [11].

The literature is rich in the electro-oxidation of CO on Pt single crystals with regular (1 0 0), (1 1 0) and (1 1 1) surfaces in acidic electrolytes [12–14]. CO adsorbed on these surfaces appears as linearly bonded species and its adsorption isotherm can be fitted with Tempkin equation [15]. The CO-poisoning effect is arisen from a blocking by CO

* Corresponding author. Tel.: +86 10 62772592; fax: +86 10 62792122.
E-mail address: bqxu@mail.tsinghua.edu.cn (B.-Q. Xu).

0008-6223/$ - see front matter © 2006 Elsevier Ltd. All rights reserved.
doi:10.1016/j.carbon.2006.05.027

of the surface sites active to hydrogen adsorption since CO molecules are bonded much more strongly and the oxidation potential of adsorbed CO is much higher than that of adsorbed hydrogen [16–18].

Three different approaches have been being attempted to mitigate the effect of CO poisoning in PEMFC technology [18]: (1) use of suitable platinum alloy electro-catalyst to increase the competitiveness of hydrogen adsorption, (2) assuming higher cell operating temperature to reduce the dynamic coverage of CO at the Pt surface, and (3) adding a small amount of oxygen into the fuel gas flow to enable a selective oxidation of CO in hydrogen. With respect to the electro-catalyst, an alternative approach to enhance the catalyst performance could be the search for suitable active supporting materials for Pt [19]. Nature of the supporting materials has proven to play an important role in enhancing the electro-catalytic activity for the oxygen reduction reaction (ORR) at the cathode and methanol oxidation reaction (MOR) at the anode catalyst [20–23].

Being a new form of carbon materials [24], carbon nanotubes (CNTs) have been a main focus of many current research efforts since recent development in large-scale syntheses of the material has significantly increased their availability [25,26]. Due to their unique structure, high surface area, low resistance and high stability, the CNTs are considered as promising supporting materials for the electro-catalyst in the PEMFC technology [27–35]. A number of earlier investigations have shown that Pt deposited on CNTs can exhibit high activity for methanol electro-oxidation as well as oxygen electro-reduction [28–35]. But, a pretreatment of the CNT support in oxidative mineral acid was always found beneficial for a homogeneous metal deposition and thus for better catalytic performance [21–23,30–33]. The oxidative pretreatment can affect the density of surface functional groups which could be necessary for better metal deposition and metal-support interaction [32,33].

A suitable electro-catalyst in the PEMFC technology should be at least less sensitive to CO poisoning than the conventional Pt/XC-72 catalyst. However, little is known about effects of the supporting carbon materials on the electro-chemical oxidation of CO. In the present study, we investigate the effects of oxidative pretreatments of CNTs in different mineral acids. The pretreated CNT samples are characterized with BET, TEM, XRD, FTIR, and electro-chemical measurements to understand the effect of supporting carbon material on the electro-catalytic oxidation of CO.

2. Experimental

2.1. Pretreatment of CNTs in oxidative acids

The multi-wall carbon nanotube (MWNT) (i.d. 3–10 nm, o.d. 6–20 nm, ratio of length to diameter 100–1000) material was received from the laboratory of Professors Wei and Luo of the Chemical Engineering Department (Tsinghua University), where the material was prepared by catalytic vapor deposition (CVD) of propylene using Fe/Al_2O_3 as the catalyst [36]. Pretreatments of the as-received CNT material were conducted by immersing the material in oxidative mineral acids, followed by refluxing at 80–90 °C for 3 h under vigorously agitation. After separation by filtration, the pretreated materials were washed extensively with deionized water and dried in air at 120 °C for 5 h. The mineral acids used for the pretreatments were 30% HNO_3, mixed 98% H_2SO_4 + 70% HNO_3 and 98% H_2SO_4 + 0.4 M $K_2Cr_2O_7$ solutions, resulting in samples denoted CNTs-I, CNTs-II and CNTs-III, respectively. Pretreatment of the well-known Vulcan XC-72 carbon with mixed 98% H_2SO_4 + 70% HNO_3 acids produced a carbon sample coded as XC-72-II.

2.2. Catalyst preparation

All the catalyst samples were prepared by Pt deposition onto the supporting carbon materials using a modified colloid method described in our earlier work [37]. Briefly, a Pt sulfite complex was first synthesized from K_2PtCl_6 and $NaHSO_3$. This Pt sulfite complex was dissolved in deionized water at pH = 3.0 and then proper amount of CNTs was added to form a CNT suspension in the solution. Under vigorous stirring and careful pH (≈3.0) control with aqueous NaOH, hydrogen peroxide was then added dropwise to induce oxidative decomposition of the sulfite complex to deposit Pt nanoparticles onto the suspended CNTs. After extensive washing, the solid from the solution was finally dried at 393 K to give the Pt/CNT catalyst. Pt loading in the catalysts was 20 wt%. The Pt/CNTs-as-received and Pt/XC-72, which represent Pt catalysts supported by CNTs-as-received and Vulcan XC-72 carbon, respectively, were prepared as reference catalysts for comparison purpose. And also, a use of the pretreated Vulcan XC-72 carbon as the catalyst support produced the Pt/XC-72-II catalyst.

2.3. Characterization and CO electro-oxidation evaluation of the catalysts

Surface areas and pore size distribution of the carbon materials and their supported Pt catalysts were measured by nitrogen adsorption at 77 K on a Micromeritics ASAP 2010C instrument. Transmission electron microscopy (TEM) was performed on a Hitachi H800 microscope operating at 150 kV to determine sample morphology and metal dispersion. Fourier transform infrared transmission spectroscopy (FTIR) was carried out on a PE 2000 FTIR spectrometer. The frequency was scanned from 400 to 1400 cm^{-1} with a total of 20 scans for each of the samples. The sample was mixed and grounded with KBr at a ratio of 1:20 (wt.) before it was pressed into a wafer for the measurement. The crystallinity of the samples was determined by X-ray diffraction (XRD) performed on a Bruker d8 diffractometer equipped with a Cu Kα radiation and a graph-

ite monochromatic operation at 45 kV and 40 mA. The diffraction patterns were scanned at a rate of 1.2 deg/min with a scan step of 0.02 deg.

The catalyst electrodes were prepared by conventional ink method. The catalyst inks were prepared by mixing 5 mg catalyst sample with 0.25 ml isopropanol, followed by adding 20 μl Nafion (5% in ethanol solution) and dispersing ultrasonically for 15 min. To prepare the working electrode, 50 μl of the ink was pasted onto the carbon paper to obtain a Pt loading of approximately 0.2 mg/cm^2. The electro-chemical measurements were carried out with 0.5 M H_2SO_4 solution as the electrolyte in a three-electrode cell at 298 K. A saturated calomel electrode (SCE) and a Pt foil were used as the reference and the counter electrodes, respectively. The cyclic voltammogram and chronoamperometry measurements were performed on a PARC EG&G M273 electro-chemical system. The electro-chemical potential data reported in this paper were calibrated to the RHE values. Unless otherwise specified, the solutions were firstly deaerated with high purity nitrogen prior to any measurement. For the CO-stripping measurement, the working electrode was repeatedly scanned in between 0 and 1.2 V at a sweep rate of 100 mV/s to assure stabilization of the electrode in 0.5 M H_2SO_4 solution. Adsorption of CO on the electrode catalyst was conducted by bubbling carbon monoxide (UHP grade) through the electrolyte (0.5 M H_2SO_4) for 15 min, followed by purging with nitrogen for 20 min to remove any residual CO from the solution. The CO-stripping CV curve and blank CV curve were obtained from two consecutive scan cycles in between 0 and 1.2 V (sweep rate: 10 mV/s). The chrono-amperometric curves of the CO electro-oxidation were measured at 0.7 V in flowing CO.

3. Results and discussion

3.1. Effects of pretreatment on the physicochemical property of CNTs

Fig. 1 shows the TEM images of the CNT samples before and after the oxidative pretreatments. All of these CNT samples are featured by hollow tubular nanostructures with diameters in between 6 and 20 nm (pore diameter: 3–10 nm) and length up to several micrometers, demonstrating no change of the structural feature of the CNTs after the different pretreatments. The as-received CNT sample (Fig. 1A) and the one pretreated with nitric acid (CNTs-I: Fig. 1B) were contaminated with some

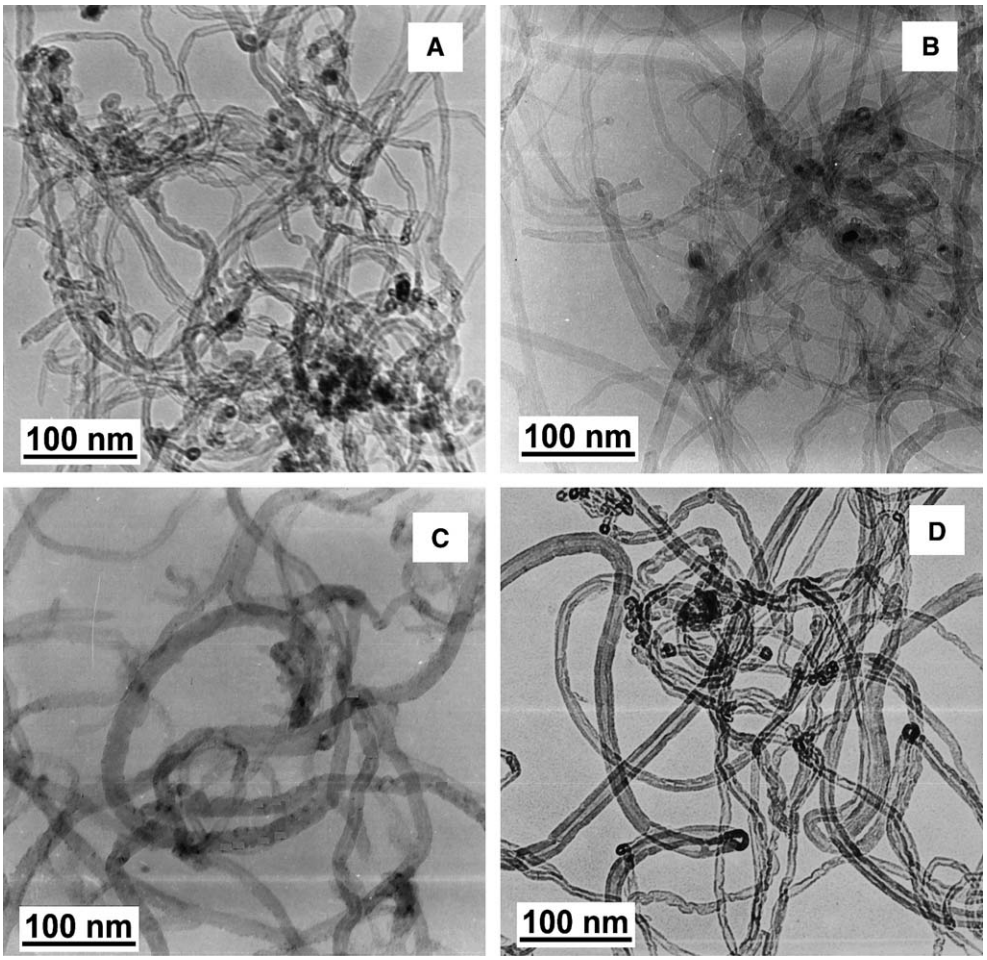

Fig. 1. TEM micrographs of the as-received (A) and activated CNTs (B–D). B, CNTs-I; C, CNTs-II; D, CNTs-III.

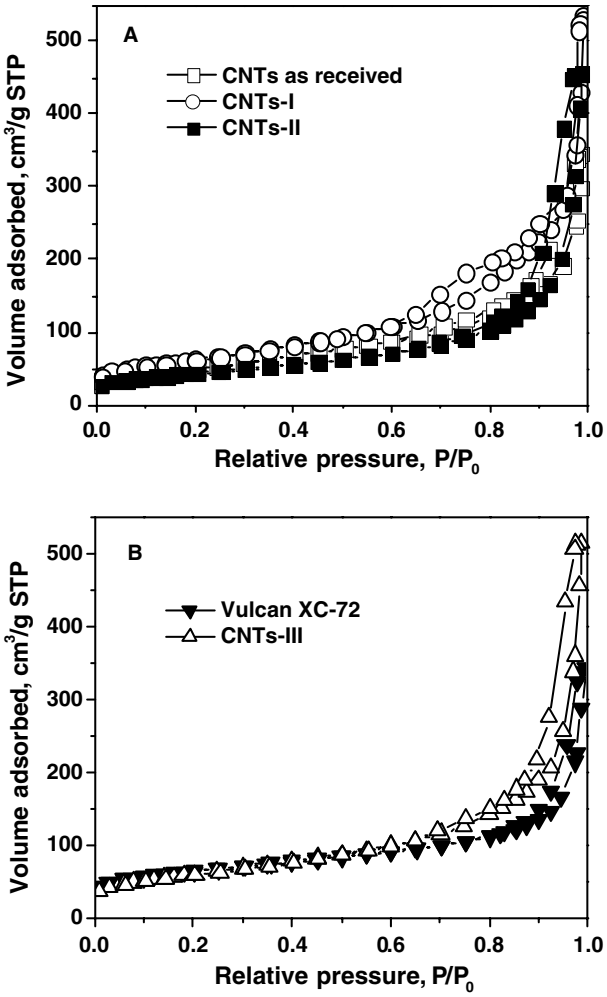

Fig. 2. Representative nitrogen adsorption–desorption isotherms of CNTs and Vulcan XC- 72.

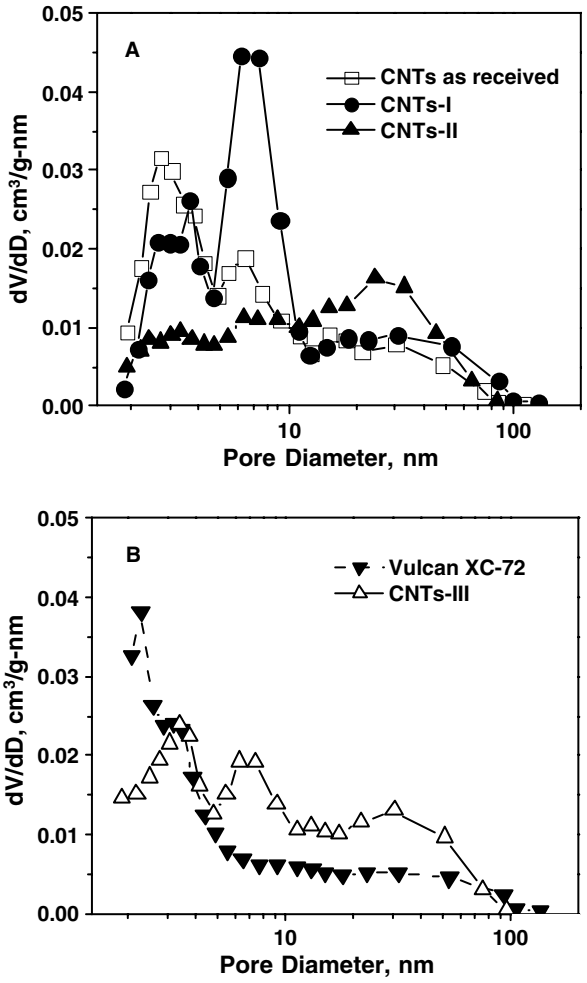

Fig. 3. Mesopore size distribution of CNTs and Vulcan XC-72.

impurities including the Fe/Al_2O_3 catalyst, which was employed in the CVD preparation of the as-received CNTs. The impurities disappeared after the sample was pretreated in either of the mixed acids, $H_2SO_4 + HNO_3$ (CNTs-II: Fig. 1C) or $H_2SO_4 + K_2Cr_2O_7$ (CNTs-III: Fig. 1D), indicating that the mixed acids were effective in eliminating the impurities from the as-received sample.

The specific surface area and porosity of the CNT samples as well as Vulcan XC-72 carbon were measured by N_2 physisorption at 77 K and the results are shown in Fig. 2 and Table 1. All the adsorption–desorption isotherms are belong to Type IV in the classification of IUPAC [38], with obviously adsorption–desorption hysteresis loop at the high pressure side. The Type-IV adsorption isotherm characterizes the existence of mesoporosity of the CNT samples, which may play an important role in the later Pt deposition processes [39]. As in many other documentations [40–44], the well-known BJH method was used to analyze the desorption branch of the isotherms at relative high pressure to obtain the pore size distribution of the CNT samples (Fig. 3). According to the definition for

Table 1
Specific surface area and porosity of CNTs and Vulcan XC-72 carbon samples

Carbon materials	S_{BET}, m^2/g	S_{meso-}, m^2/g	V_{total}, cm^3/g	V_{meso-}, cm^3/g
Vulcan XC-72	216	137	0.60	0.57
CNTs as-received	175	150	0.38	0.37
CNTs-I	221	194	0.53	0.52
CNTs-II	156	137	0.43	0.42
CNTs-III	217	200	0.52	0.51

micropores (below 2 nm), mesopores (between 2 and 50 nm), and macropores (above 50 nm) [44], microporosity is significant in the Vulcan XC-72 carbon while mesoporosity dominates in all of the CNT samples. Within the CNT samples, it is easy to see that the pore size distribution was significantly affected by the pretreatment condition (Fig. 3 and Table 1). In comparison with the as-received CNTs without any pretreatment, the percentage of pores within 10–50 nm was significantly enhanced in CNTs-II and CNTs-III, while in CNTs-I the pores with sizes in between 5 and 10 nm were increased pronouncedly. The fact that the increased porosity in CNTs-I (Fig. 3A) was contributed

by those pores with sizes (5–10 nm) slightly smaller than the diameters of carbon tubes in the CNT material (Fig. 1) suggests that the pretreatment with 30% HNO_3 effected opening of the closed ends of the carbon tubes. On the other hand, the increased porosity at 10–50 nm in CNTs-II and CNTs-III would indicate a disentanglement of the entangled carbon nanotubes by the pretreatments with the mixed $HNO_3 + H_2SO_4$ and $H_2SO_4 + K_2Cr_2O_7$. Recently, Rolison et al. [44,45] reported that molecules within microporous channels could suffer significantly hindered transport, while molecules in mesoporous channels can approach diffusion rates comparable to those in an open medium. Therefore, in terms of the pore structure, the mesoporous CNTs would be more optimistic as the supporting material for electro-catalysts.

The specific BET surface areas of these carbon samples are calculated by the BET equation and the total pore volumes are obtained from the amount of nitrogen adsorbed at a relative pressure of 0.99 at 77 K. As listed in Table 1, the total pore volumes of the CNT materials increased after the pretreatments due to the removal of impurities either inside the canals or at the ends of the carbon nanotubes.

FTIR was used to detect the overall change of functional groups on the surface of CNTs before and after the oxidative pretreatments, the results are shown in Fig. 4. In comparison with the other samples, much stronger absorption bands were found at 1000–1200 cm^{-1} for CNTs-II. According to Ref. [46], these results indicate that a high density of surface functional groups, such as C—OH and —C=O, are created on the surface of CNTs after the pretreatment in the mixed $HNO_3 + H_2SO_4$ acids. However, no significant formation of surface functional groups was detected in CNTs-I and CNTs-III. It is interesting to see that the functional groups of CNTs-II were similar by nature to those of the starting as-received CNTs, although their densities were much lower in the later sample. A referee questioned about that the functional groups of the as-received CNTs might affect the formation of surface functional groups during the oxidative pretreatments. This is an interesting point that needs to be clarified in future work.

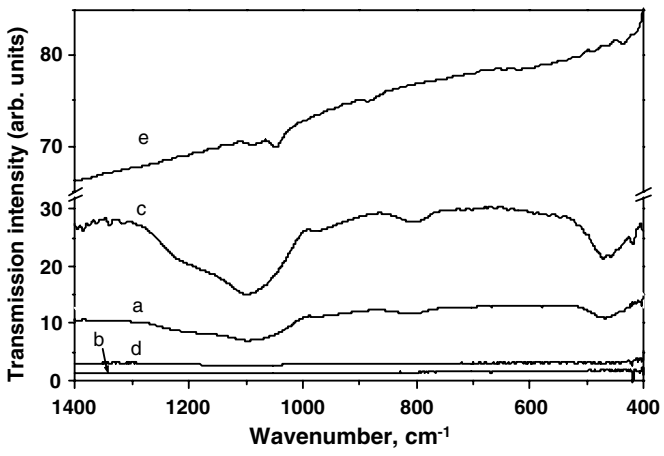

Fig. 4. FTIR spectra of CNTs and Vulcan XC-72: (a) CNTs-as-received; (b) CNTs-I; (c) CNTs-II; (d) CNTs-III; (e) Vulcan XC-72.

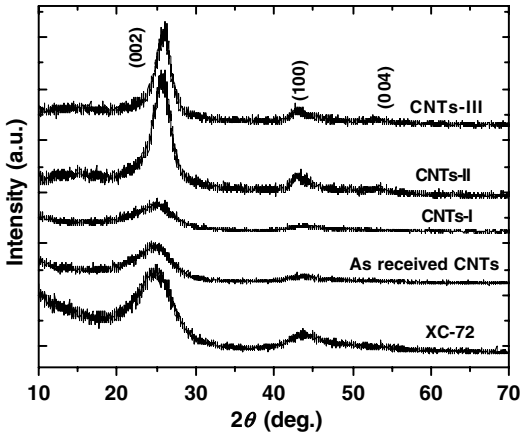

Fig. 5. X-ray diffraction (XRD) patterns of various carbon supports.

Fig. 5 compares the XRD patterns of the carbon materials used in the present study. The samples pretreated with the mixed acids (i.e., CNTs-II and CNTs-III) exhibited excellent graphitic crystallinity by showing clear diffraction peaks associated with the (002), (100) and (004) planes. XC-72 carbon, CNTs-I and the as-received CNTs seem to contain significant amorphous features because they showed exceptionally wide diffraction peaks from the (002) and (100) planes. It has been reported [47] that the graphitic crystallinity of the carbon support is important for electron transport in the electro-chemical reactions due to its good electronic conductivity and interaction with the supported metal catalyst. Hence, in terms of electronic conductivity, CNTs-II and CNTs-III could be more effective supporting materials for Pt electro-catalyst.

To summarize, the morphology, crystallinity and surface properties of CNTs are modified by the pretreatments with oxidative mineral acids. In particular, the pretreatment of the as-received CNTs with mixed $HNO_3 + H_2SO_4$ acids produced sample CNTs-II having fairly large mesoporosity at pore sizes larger than 10 nm, higher concentration of surface functional groups and good graphitic crystallinity.

3.2. Morphology of the Pt/CNT electro-catalysts

Fig. 6 shows the typical TEM images of Pt particles deposited on Vulcan XC-72 and the CNT materials. The large light gray particles and tubes are the images of the carbon materials (A for Vulcan XC-72; B–E for CNTs in Fig. 6) while the scattered black spots are the images of Pt particles. With the aid of filter technology and tilting operation of TEM, we found that Pt particles were deposited on both the inner and outer surfaces of the carbon nanotubes in the Pt/CNT catalysts. The bar graphs located on the right of the TEM images in Fig. 6 show the size distribution of Pt particles, obtained by randomly measuring the sizes of at least 150 particles in the magnified TEM

images. The averaged size of Pt particles in each of the Pt loaded samples is listed in the last column of Table 2. Irrespective of the pretreatments of CNTs, the averaged Pt particle sizes (≈3 nm) in all Pt/CNT catalysts were found quite close to that in Pt/XC-72 catalyst. However, the size distribution was narrower (1–5 nm) in Pt/XC-72 and Pt/CNTs-III than those in other Pt/CNT catalysts (1–8 nm).

3.3. Electro-chemical oxidation of CO on Pt/CNT electro-catalysts

Fig. 7 shows the CO-stripping and background voltammograms of the Pt/CNT catalysts in 0.5 M H_2SO_4 solution at a sweep rate of 10 mV/s. The results of Pt/XC-72 are also included in this figure for comparison. It is seen that the background current, associated with the double-layer capacitance, of the electrode with Pt/CNTs-as-received is much lower than those with Pt/CNTs-I, -II and -III, possibly due to poor mesoporosity and smaller percentage of accessible surface in Pt/CNTs-as-received [28]. The clear peaks at the low potential side (0.1–0.3 V) proved the occurrence of hydrogen adsorption on the Pt catalysts. Blank CO-stripping measurements with either pretreated or non-pretreated CNTs, instead of Pt/CNT catalysts, for the electrode demonstrated no adsorption of CO on the surface of the CNT materials. Therefore, the peaks in

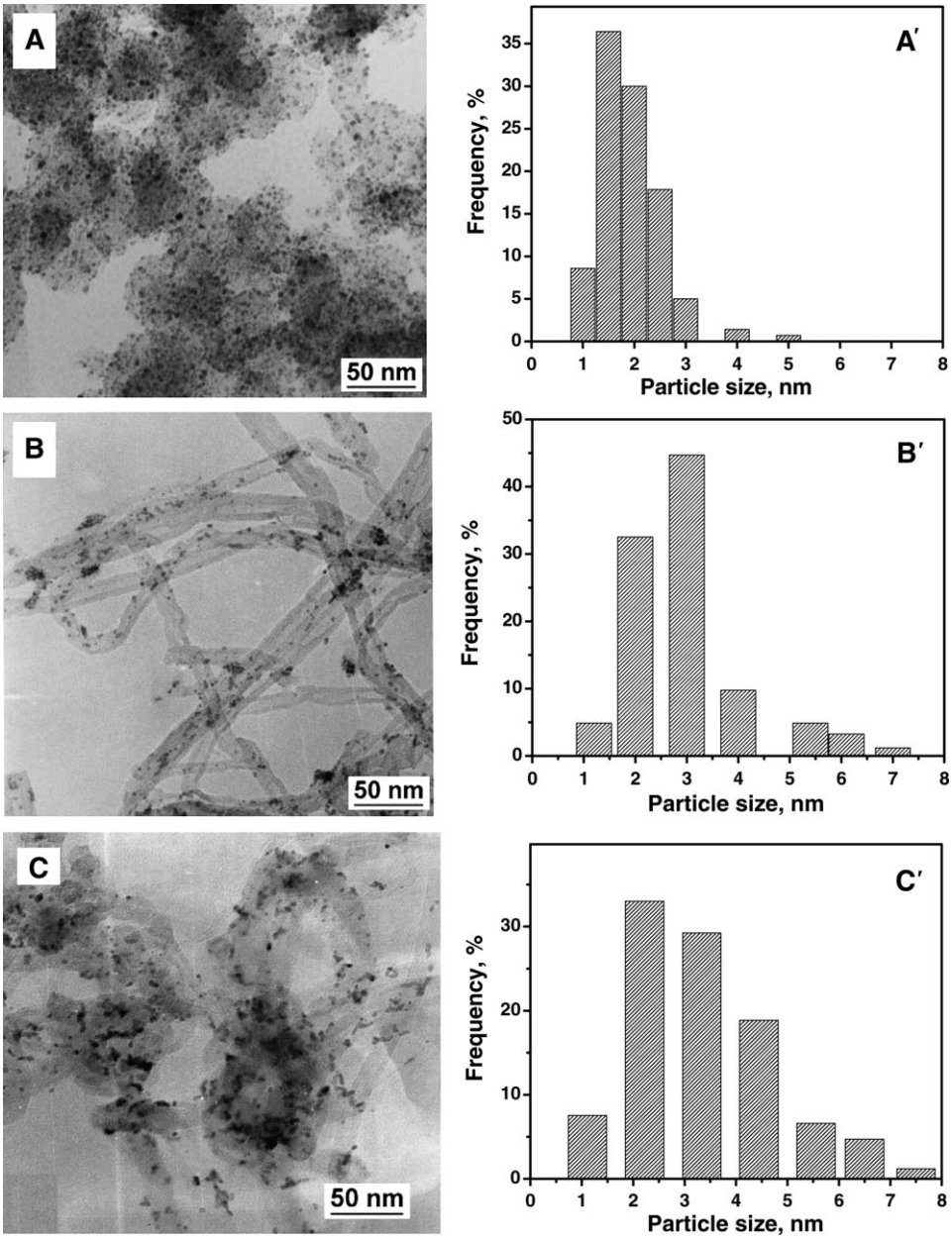

Fig. 6. TEM micrographs of Pt/XC-72 (A), Pt/CNTs-as-received (B), Pt/CNTs-I (C), Pt/CNTs-II (D) and Pt/CNTs-III (E); the particle size distribution of metallic Pt in the samples are shown by the corresponding graphs (A′–E′) located beside the TEM micrographs.

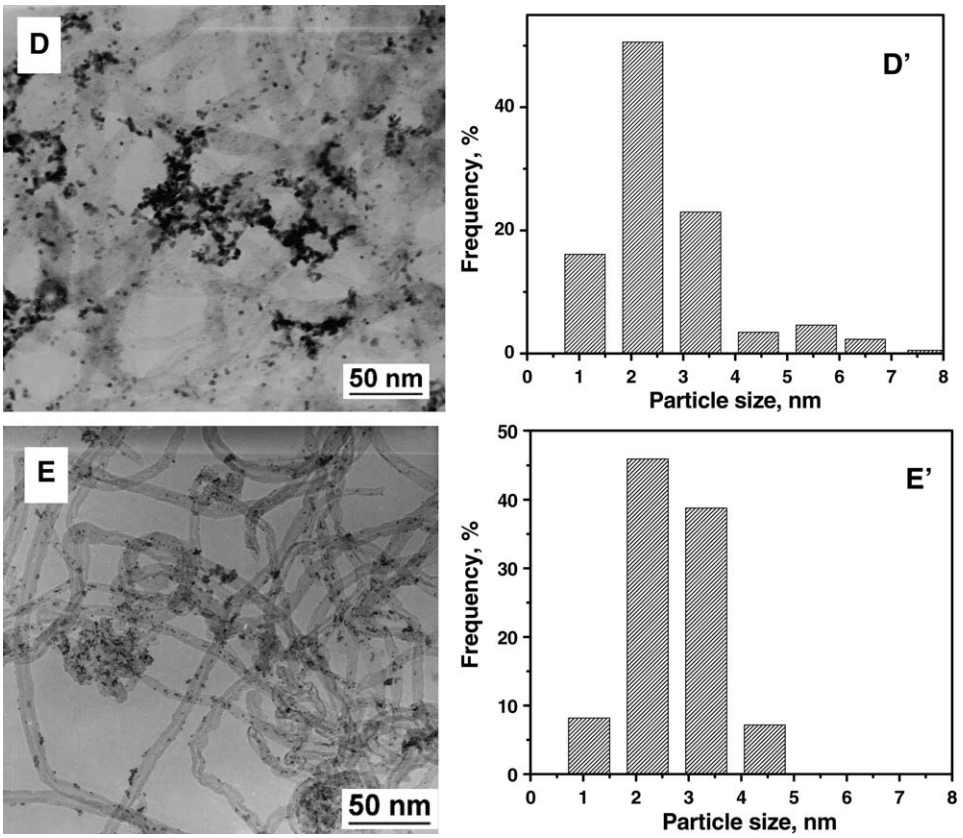

Fig 6. *(continued)*

Table 2
CO electro-oxidation by CO-stripping studies over Pt/CNTs and Pt/XC-72 catalysts

Catalysts	Onset potential, V vs RHE	Peak potential, V vs RHE	ECA, m^2/g	Areal specific activity at 0.65 V (mA/cm^2 Pt)	TOF at 0.65 V, s^{-1}	Particle size, nm
Pt/XC-72	0.65	0.82	74.4	0.0013	0.003	2.5 ± 0.5
Pt/XC-72-II	0.65	0.79	32.1	0.0060	0.014	–
Pt/CNTs-as-received	0.56	0.71, 0.81	15.6	0.0083	0.020	3.2 ± 0.5
Pt/CNTs-I	0.57	0.72, 0.81	24.4	0.0102	0.024	3.0 ± 0.5
Pt/CNTs-II	0.51	0.68, 0.74	30.9	0.0285	0.068	2.8 ± 0.5
Pt/CNTs-III	0.61	0.78	52.6	0.0049	0.012	2.6 ± 0.3

CO-stripping measurements of Fig. 7 are undoubtedly associated with the electro-oxidation of CO molecules adsorbed on the Pt catalysts. The disappearance of the hydrogen adsorption peaks at low potentials on the CO-stripping curves indicates blocking of the hydrogen adsorption sites by CO adsorption, i.e., CO-poisoning, in the Pt/CNT and Pt/XC-72 electrode catalysts. The onset potentials of CO electro-oxidation on the different Pt/CNT catalysts appeared in between 0.5 and 0.6 V, which are significantly lower than the onset potential (0.7 V) on Pt/XC-72 catalyst. Also, the CO oxidation peaks on every Pt/CNT catalyst were negatively shifted by 40–160 mV in comparison with the one on the Pt/XC-72 catalyst (Fig. 7 and Table 2), indicating that all of the Pt/CNT catalysts are more tolerant to CO poisoning. Moreover, it is noticeable that the catalyst Pt/CNTs-II gave the lowest onset (0.51 V) and peak (0.68 V) potentials and showed also the highest areal specific activity for the electro-oxidation of CO.

A referee reminded us that the Vulcan XC-72 carbon in the reference Pt/XC-72 catalyst was not pretreated in the oxidative acids; the same pretreatment as for CNTs-II must be conducted in order to compare the resistibility to CO-poisoning of Pt/CNT-II and Pt/XC-72. Pretreatment of Vulcan XC-72 carbon with mixed 98% H_2SO_4 + 70% HNO_3 acids was then conducted and the pretreated carbon sample was named as XC-72-II. We then obtained a Pt/XC-72-II catalyst by deposition of Pt onto this pretreated carbon support XC-72-II. The CO-stripping CV curve of this Pt/XC-72-II catalyst was also included in Fig. 7 and

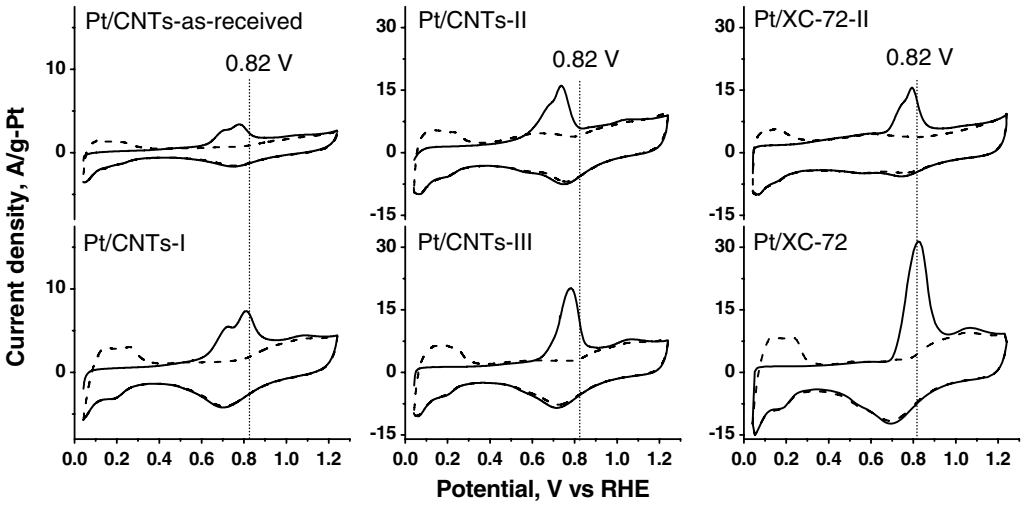

Fig. 7. CO-stripping curves of Pt/CNTs and Pt/XC-72 samples in 0.5 M H_2SO_4 solution at 298 K with the sweep rate of 10 mV/s; the dashed lines show the background voltammogram curves before the CO adsorption.

the parameters derived from the CO-stripping measurement on this catalyst added to Table 2 to compare with the other catalysts. Clearly, the onset (0.65 V) and peak (0.79 V) potentials of the CO electro-oxidation over Pt/XC-72-II are very close to those over its counterpart Pt/XC-72 catalyst, thus suggesting that the pretreatment of XC-72 carbon in the mixed 98% H_2SO_4 + 70% HNO_3 acids has little effect on the electro-oxidation of CO, although Pt/XC-72-II showed a much lower ECA than its counterpart Pt/XC-72 catalyst. Still, the onset (0.51 V) and peak (0.68 V) potentials over the catalyst Pt/CNTs-II appear to be the lowest.

Based on the electro-chemical area (ECA) obtained from the hydrogen adsorption peaks on the background voltammogram, and the areal specific activity (mA/cm^2) of the Pt catalyst for the CO electro-oxidation, we calculated the catalytic CO turnover frequency (TOF) on surface Pt atoms at a given working potential (0.65 V), the results are given in Table 2. It appears that the intrinsic catalytic activity by the TOF rate is in the order of Pt/CNTs-II > Pt/CNTs-I $\geqslant$ Pt/CNTs-as-received > Pt/CNTs-II $\cong$ Pt/CNTs-III > Pt/XC-72. Quantitatively, the TOF rate on the Pt/CNTs-II catalyst was approximately five times that of Pt/XC-72-II but approximately 20 times that of Pt/XC-72 catalyst.

Therefore, the catalyst Pt/CNTs-II is unique in showing the lowest onset and peak potentials (Fig. 7) as well as the highest TOF rate for the electro-oxidation of CO (Table 2). These results suggested that the catalyst Pt/CNTs-II would be the most CO tolerant among the catalysts used in the present work. Xin et al. [22,23] and He et al. [28,29] found that Pt/CNTs exhibited enhanced activities and cell performance for the reduction of oxygen when it was used as the cathode catalyst.

The high graphitic crystallinity and high density of surface functional groups of the support CNTs-II would be responsible for the high resistibility to CO-poisoning of the catalyst Pt/CNTs-II since they could function to anchor the metallic catalyst and to strengthen the metal-support interaction [4] that would be beneficial for electron transfer in between the metal and supporting carbon material during the electro-chemical reaction. Electron transfer between Pt and carbon support was actually detected in an electron spin resonance (ESR) study of Baschuk and Li [3], who showed that the amount of unpaired electrons in Pt/C was much less than those in unsupported Pt black catalysts.

According to Refs. [12–14,18], electro-oxidation of CO would be possible only when there is formation of $Pt—OH_{ads}$ at surface of the Pt catalyst:

$$Pt + H_2O \rightarrow Pt—OH_{ads} + H^+ + e \quad (1)$$

Theoretically, the potential required for the formation of $Pt—OH_{ads}$ in the acid media is approximately 0.62 V at 25 °C [48]. With the presence of OH_{ads} ($Pt—OH_{ads}$), the electro-oxidation of adsorbed CO on the Pt surface can be expressed as [37]:

$$Pt—CO + Pt—OH_{ads} \rightarrow 2Pt + CO_2 + H^+ + e \quad (2)$$

Since the onset potentials of CO electro-oxidation are lower than 0.62 V on the present Pt/CNT catalysts, some active —OH groups or their equivalent might have been provided by the supporting CNTs, which would be partly the reason why the onset potentials of CO oxidation on Pt/CNT catalysts were reduced in comparison with the Pt/XC-72 catalysts. Further work will be needed to confirm this explanation.

Two well-separated CO oxidation peaks are observed in Fig. 7 on the catalyst samples except Pt/CNTs-III and the two Pt/XC-72 catalysts, indicating that two types of surface sites were available for CO adsorption. The presence of two types of surface sites for CO adsorption are consistent with Becdelievre et al. [12], who discriminated the CO adsorption species associated with the two types of surface sites by reversing the potential sweep just before the appearance of the second CO electro-oxidation peak. The

hydrogen adsorption–desorption signals on the subsequent potential sweep curve revealed that those adsorbed CO molecules associated with the second electro-oxidation peak were blocking the surface sites on which hydrogen atoms remained strongly adsorbed [12]. In other words, adsorbed CO molecules associated with the first CO electro-oxidation peak (i.e., the one on the low potential side) would block the surface sites that adsorb hydrogen with relative weak bonding. The studies performed by Beden and Lamy [13] on the electrodes with single crystals of Pt (1 1 1) and Pt (1 0 0) catalysts produced similar conclusions. Beden and Lamy also showed that the oxidation of CO on Pt (1 1 1) surface occurred at potential 50 mV lower than that on the Pt (1 0 0) surface. Thus, the peak at the lower potential of the present study could be associated with the electro-oxidation of the CO molecules adsorbed on the exposed (1 1 1) surface while that at higher potential with those bonded to the exposed (1 0 0) surface. According to in situ IR absorption studies in Refs. [13,14], the second peak at higher potential was connected with strongly adsorbed CO molecules, which means that CO adsorption on Pt(1 1 1) is weaker than it does on Pt(1 0 0) surface. On the other hand, the interaction strength of CO with the Pt catalyst could be dependent of the particle size of Pt, e.g., Mukerjee and Mcbreen et al. [49] showed that the strength of Pt—CO bond would increase as the Pt particle size became smaller than 5 nm. The single CO oxidation peak at the higher potential side (0.82 V) on Pt/CNTs-III and Pt/XC-72 electrodes seems in consistent with the Pt particle size effect on the bonding of CO at the Pt surface since Pt particles in these two catalysts were smaller than 5 nm (Fig. 6). Thus, the existence of Pt particles larger than 5 nm in the other Pt/CNT catalysts (Pt/CNTs-I, Pt/CNTs-II and Pt/CNTs-as-received) may be responsible for the first electro-oxidation peak of CO in Fig. 7. Hence, it is inferred that the preferred exposed catalyst surface is dominant by Pt (1 0 0) sites when the Pt particles are smaller than 5 nm but the surface becomes dominant by Pt (1 1 1) sites when the particles become larger.

Chronoamperometry measurements were carried out to evaluate the catalyst stability in the electro-oxidation of CO and the results are shown in Fig. 8. The current densities on all the electro-catalysts reduced sharply in the very initial minutes, followed by a gentle decrease to approach constant values after 15–20 min. This sharp decrease in the current density is most likely due to the exceptionally high surface coverage of CO at the beginning of the electro-oxidation reaction. The gentle decrease period would mean a transition in approaching a dynamically equilibrated CO coverage on the Pt catalyst. Then, the constant current density at longer reaction time would characterize a steady state of the adsorption and oxidative stripping of CO.

Therefore, the constant current densities in Fig. 8 can be used to evaluate the steady state catalytic activities of the electro-catalysts, which can be ranked in the order of Pt/CNTs-II > Pt/CNTs-as-received ⩾ Pt/CNTs-III > Pt/CNTs-I ⩾ Pt/XC-72. This order is somewhat different from the one (i.e., Pt/CNTs-II > Pt/CNTs-I ⩾ Pt/CNTs-as-received > Pt/CNTs-III > Pt/XC-72) obtained in the CO-stripping CV measurements (Table 2), but both the chronoamperometry and CO-stripping CV measurements reveal that Pt/CNTs-II is the most active while Pt/XC-72 the least effective electro-catalyst for the electro-oxidation of CO.

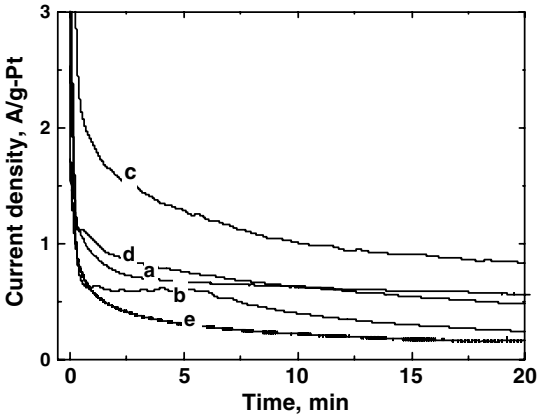

Fig. 8. *I–t* plots of CO electro-oxidation at 0.7 V over Pt/CNTs-as-received (a), Pt/CNTs-I (b), Pt/CNTs-II (c), Pt/CNTs-III (d), and Pt/XC-72 (e) catalysts.

On the other hand, electro-oxidation of CO on the electrode catalyst is affected by a number of steps at the molecular levels, including mass transfer (diffusion), adsorption, and surface electro-chemical oxidation and desorption. The electro-oxidation of adsorbed CO on Pt surface is undoubtedly a much slower step in comparison with the adsorption and desorption steps according to Ref. [13]. However, influence of CO diffusion on the electro-oxidation reaction is not yet clear. By varying the CO flowing (bubbling) rate during the chronoamperometry measurement, we investigated the CO diffusion effect over the catalysts Pt/CNTs-II and Pt/XC-72, respectively. Fig. 9 shows that the current

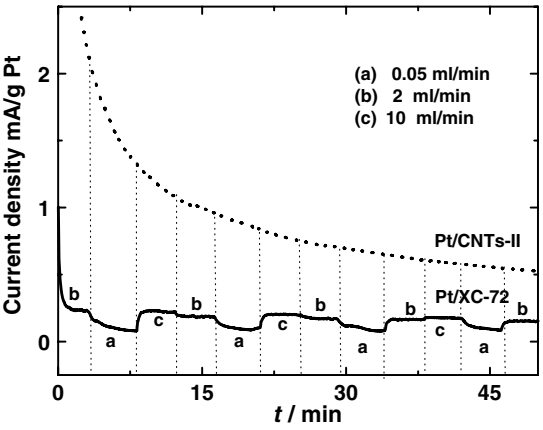

Fig. 9. The effect of CO flowing (bubbling) rate on the current of CO electro-oxidation at 0.7 V over Pt/CNTs-II and Pt/XC-72 catalysts: (a) 0.05 ml/min, (b) 2 ml/min, (c) 10 ml/min.

density on the least active conventional Pt/XC-72 electro-catalyst was apparently affected by the CO flowing/bubbling rate, e.g., the current density was enhanced from 0.09 to 0.25 mA (≈3 times) when the CO flowing/bubbling rate was increased from 0.05 ml/min to 10 ml/min (200 times). In contrast, the current density on the most active Pt/CNTs-II electro-catalyst did not change during the variation of the CO flowing/bubbling rate. These results indicate clearly a significant CO diffusion effect on the electro-oxidation reaction with the conventional Pt/XC-72 catalyst but the effect can reasonably be neglected with the catalyst Pt/CNTs-II. The absence of CO diffusion effect on Pt/CNTs-II can be well accounted for by the dominant mesoporosity in its support material CNTs-II. It is therefore conclusive that mesoporosity of the supporting carbon material is also an important factor in effecting Pt catalyst for the electro-chemical oxidation of CO.

4. Conclusions

The morphology, crystallinity and surface properties of CNTs were modified by the pretreatments with oxidative mineral acids (HNO_3, mixed $HNO_3 + H_2SO_4$ and $H_2SO_4 + K_2Cr_2O_7$). In particular, pretreatment of the as-received CNTs with mixed $HNO_3 + H_2SO_4$ acids produced material CNTs-II having fairly large mesoporosity at pore sizes larger than 10 nm, higher concentration of surface functional groups and good graphitic crystallinity. The deposition of 20% Pt on the pretreated CNT supports by modified colloidal method led to Pt/CNT catalysts with average Pt particle size at approximately 3.0 nm.

The CO-stripping CV measurements showed that the Pt/CNT catalysts are more tolerant to CO poisoning since the CO electro-oxidation peak potentials over these Pt/CNT catalysts are 40–160 mV lower than that over the conventional Pt/XC-72 catalyst. The Pt/CNTs-II appeared to be the most CO tolerant catalyst since it showed the lowest onset (0.51 V) and peak (0.68 V) potentials on the CO-stripping curves; this catalyst also gave the highest catalytic TOF rate for CO electro-oxidation at 0.65 V. The steady state chronoamperometric measurements also confirmed that the catalyst Pt/CNTs-II is the most active catalyst for the electro-oxidation of CO.

Acknowledgements

The authors acknowledge the financial support of this work from NSF (Grants: 20590362) and the Ministry of Science and Technology (Grant: G2000026408) of China. We thank also the Analytic Foundation of Tsinghua University for partial support of the TEM measurements.

References

[1] Gasteiger HA, Markovic N, Ross PN, Cairns EJ. CO electrooxidation on well-characterized Pt—Ru alloys. J Phys Chem 1994;98(2):617–25.

[2] Mukerjee S, Urian RC. Bifunctionality in Pt alloy nanocluster electrocatalysts for enhanced methanol oxidation and CO tolerance in PEM fuel cells: electrochemical and in situ synchrotron spectroscopy. Electrochim Acta 2002;47(19):3219–31.

[3] Baschuk JJ, Li X. Carbon monoxide poisoning of proton exchange membrane fuel cells. Int J Energy Res 2001;25(8):695–713.

[4] Yin SF, Xu BQ, Zhou XP, Au CT. A mini-review on ammonia decomposition catalysts for on-site generation of hydrogen for fuel cell applications. Appl Catal A 2004;277(1–2):1–9.

[5] Thomas CE, James BD, Lomax FD, Kuhn IF. Fuel options for the fuel cell vehicle hydrogen, methanol or gasoline? Int J Hydrogen Energy 2000;25(6):551–67.

[6] Wiese W, Emonts B, Peters R. Methanol steam reforming in a fuel cell drive system. J Power Sources 1999;84(2):187–93.

[7] Korotkikh O, Farrauto R. Kinetics of the selective low-temperature oxidation of CO in H_2-rich gas over Au/α-Fe_2O_3. Catal Today 2000;62(2–3):249–54.

[8] Kahlich MJ, Gasteiger HA, Behm RJ. Kinetics of the selective low-temperature oxidation of CO in H_2-rich gas over Au/α-Fe_2O_3. J Catal 1999;182(2):430–40.

[9] Divisek J, Oetjen HF, Peinecke V, Schmidt VM, Stimming U. Components for PEM fuel cell systems using hydrogen and CO containing fuels. Electrochim Acta 1998;43(24):3811–5.

[10] Yu HM, Hou ZJ, Yi BL, Lin ZY. Composite anode for CO tolerance proton exchange membrane fuel cells. J Power Sources 2002;105(1):52–7.

[11] Watkins DS. Research, development and demonstration of solid polymer fuel cell systems. In: Blomen L, Mugerwa M, editors. Fuel cell systems. New York: Plenum Press; 1993. p. 493.

[12] de Becdelièvre AM, de Becdelievra J. Electrochemical oxidation of adsorbed carbon monoxide on platinum spherical single crystals. J Electroanal Chem 1990;294:97–110.

[13] Beden B, Lamy C. The electrooxidation of CO – a test reaction in electrocatalysis. Electrochim Acta 1990;35:691–704.

[14] Kazarinov VE, Andreev VN, Shlepakov AV. Composition and properties of the adsorption products of CO and CO_2 on platinized platinum. Electrochim Acta 1989;34(7):905–13.

[15] Dhar HP, Christner LG, Kush AK. Nature of CO adsorption during H_2 oxidation in relation to modeling for CO poisoning of a fuel-cell anode. J Electrochem Soc 1987;134:3021–6.

[16] Vogel W, Lundquist J, Ross P, Stonehart P. Reaction pathways and poisons. 2: rate controlling step for electrochemical oxidation of hydrogen on Pt in acid and poisoning of reaction by CO. Electrochim Acta 1975;20:79–93.

[17] Sakellaropoulos G. Advances in catalysis, vol. 30. New York: Academic Press; 1981. p. 267.

[18] Hoogers G, Thompsett D. Catalysis in proton exchange membrane fuel cell technology. Cattech 2000;3(2):106–24.

[19] Lasch K, Hayn G, Jörissen L, Garche J, Besenhardt O. Mixed conducting catalyst support materials for the direct methanol fuel cell. J Power Sources 2002;105(2):305–10.

[20] Tang H, Chen JH, Huang ZP. High dispersion and electrocatalytic properties of platinum on well-aligned carbon nanotube arrays. Carbon 2004;42(1):191–7.

[21] Yu JS, Kang S, Yoon SB, Chai G. Fabrication of ordered uniform porous carbon networks and their application to a catalyst supporter. J Am Chem Soc 2002;124(32):9382–3.

[22] Li WZ, Liang CH, Qiu JS, Xin Q. Carbon nanotubes as support for cathode catalyst of a direct methanol fuel. Carbon 2002;40(5):791–4.

[23] Li WZ, Liang CH, Zhou WJ, Xin Q. Preparation and characterization of multiwalled carbon nanotube-supported platinum for cathode catalysts of direct methanol fuel cells. J Phys Chem B 2003;107(26):6292–9.

[24] Iijima S. Helical microtubules of graphitic carbon. Nature 1991;354(6348):56–7.

[25] Ebbesen TW, Ajayan PM. Large-scale synthesis of carbon nanotubes. Nature 1992;358(6383):220–2.

[26] Li WZ, Xie SS, Qian LX, Chang BH, Zou BS, Zhou WY, et al. Large-scale synthesis of aligned carbon nanotubes. Science 1996; 274(5293):1701–3.
[27] Ebbesen TW, Lezec HJ, Hiura H, Bennett JW, Ghaemi HF, Thio T. Electrical conductivity of individual carbon nanotubes. Nature 1996;382(6586):54–6.
[28] Pyun SI, Rhee CK. An investigation of fractal characteristics of mesoporous carbon electrodes with various pore structures. Electrochim Acta 2004;49(24):4171–80.
[29] He ZB, Chen JH, Liu DY, Zhou HH, Kuang YF. Electrodeposition of Pt—Ru nanoparticles on carbon nanotubes and their electrocatalystic properties for methanol electrooxidation. Diam Relat Mater 2004;13:1764–79.
[30] Che GL, Lakshmi BB, Martin CR, Fisher ER. Metal-nanocluster-filled carbon nanotubes: catalytic properties and possible applications in electrochemical energy storage and production. Langmuir 1999; 15(3):750–8.
[31] Joo SH, Choi SJ, Oh I, Kwak J, Liu Z, Terasaki O, et al. Ordered nanoporous arrays of carbon supporting high dispersions of platinum nanoparticles. Nature 2001;412(6848):169–72.
[32] Liu ZL, Lin XH, Lee JY, Zhang W, Han M, Gan LM. Preparation and characterization of platinum-based electrocatalsyts on multi-walled carbon nanotubes for proton exchange membrane fuel cells. Langmuir 2002;18(10):4054–60.
[33] Yu RQ, Chen LW, Liu QP, Lin JY, Tan KL, Ng SC, et al. Platinum deposition on carbon nanotubes via chemical modification. Chem Mater 1998;10(3):718–22.
[34] Liu ZL, Lee JY, Chen WX, Han M, Gan LM. Physical and electrochemical characterizations of microwave-assisted polyol preparation of carbon-supported PtRu nanoparticles. Langmuir 2004; 20(1):181–7.
[35] Sun X, Li R, Villers D, Dodelet JP, Desilets S. Composite electrodes made of Pt nanoparticles deposited on carbon nanotubes grown on fuel cell backings. Chem Phys Lett 2003;379(1–2):99–104.
[36] Wang Y, Wei F, Luo GH, Yu H, Gu GS. The large-scale production of carbon nanotubes in a nano-agglomerate fluidized-bed reactor. Chem Phys Lett 2002;364(5–6):568–72.
[37] Li L, Wang HX, Xu BQ, Li JL, Xing W, Mao ZQ. Studies on PEMFC electrocatalysts: physicochemical characterization of home-made Pt/C electrocatalyst. Acta Phys – Chim Sin 2003;19(4):342–6.
[38] Sing KSW, Everett DH, Haul RAW, Moscou L, Pierotti RA. Reporting physisorption data for gas solid systems with special reference to the determination of surface-area and porosity. J Rouquérol Pure Appl Chem 1985;157:603–19.
[39] Sobkowski J, Czerwinski A. Voltammetric study of carbon monoxide and carbon dioxide adsorption on smooth and platinized platinum electrodes. J Phys Chem 1985;89(2):365–9.
[40] Staszczuk P, Matyjewicz M, Kowalska E, Radomska J, Byszewski P, Kozlowski M. Studies of surface properties and fractal dimensions of carbon nanotubes using complex methods. Rev Adv Mater Sci 2003; 5:471–6.
[41] Su F, Li X, Lv L, Zhao XS. Ordered mesoporous carbon particles covered with carbon nanotubes. Carbon 2006;44:799–823.
[42] Bekyarova E, Kaneko K, Yudasaka M, Kasuya D, Iijima S, Huidobro A, et al. Controlled opening of single-wall carbon nanoborns by heat treatment in carbon dioxide. J Phys Chem B 2003; 107(19):4479–84.
[43] An KH, Yang C-M, Park JS, Jeong SY, Lee YH. Intercalant-induced superbundle formation of single-wall carbon nanotubes. J Phys Chem B 2005;109(20):10004–8.
[44] Rolison DR. Catalytic nanoarchitectrues – the importance of nothing and the unimportance of periodicity. Science 2003;299(5613): 1698–701.
[45] Anderson ML, Stroud RM, Rolison DR. Enhancing the activity of fuel-cell reactions by designing three-dimensional nanostructured architectures: catalyst-modified carbon–silica composite aerogels. NanoLetters 2002;2(3):235–40.
[46] Lambert JB, Shurvell HF, Lightner DA, Cooks RG. Organic structural spectroscopy. Upper Saddle River (NJ): Prentice-Hall; 1998. p. 205.
[47] Park KW, Sung YE, Han S, Yun Y, Hyeon T. Origin of the enhanced catalytic activity of carbon nanocoil-supported PtRu alloy electrocatalysts. J Phys Chem B 2004;108(3):939–44.
[48] Zhang HB, Lin GD, Zhou ZH, Dong X, Chen T. Raman spectra of MWCNTs and MWCNT-based H_2-adsorbing system. Carbon 2002; 40(13):2429–36.
[49] Mukerjee S, Mcbreen J. Effect of particle size on the electrocatalysis by carbon-supported Pt electrocatalysts: an in situ XAS investigation. J Electroanl Chem 1998;448(2):163–71.